Frontiers of Information Technology & Electronic Engineering
www.jzus.zju.edu.cn; engineering.cae.cn; www.springerlink.com
ISSN 2095-9184 (print); ISSN 2095-9230 (online)
E-mail: jzus@zju.edu.cn

Miniaturized UWB multi-resonance patch antenna loaded with novel modified H-shape SRR metamaterial for microspacecraft applications

Parul DAWAR‡[1], N. S. RAGHAVA[2], Asok DE[2]

([1]*Department of Electronics and Communication Engineering, Guru Tegh Bahadur Institute of Technology, GGSIPU, Delhi 110064, India*)

([2]*Department of Electronics and Communication Engineering, Delhi Technological University, Delhi 110064, India*)

E-mail: paru.dawar@gmail.com; nsraghava@gmail com; asok.de@gmail.com

Received Apr. 26, 2016; Revision accepted Aug. 14, 2016; Crosschecked Nov. 24, 2017

Abstract: We present the design and analysis of a novel modified H-shaped split ring resonator (SRR) metamaterial. It has negative permeability and permittivity characteristics with multi-band resonance for the X, Ku, and Ka frequency bands. Different configurations of the patch antenna have been analyzed with different orientations and positions of the metamaterial. Optimized performance was achieved with the new shape of the metamaterial antenna with an appreciable 9 dB gain, 77 GHz bandwidth, 100% radiation efficiency, and 65% reduction in active area. The second-order fractal metamaterial antenna achieves high miniaturization on the order of 1/21. This is truly a boon in the communications world, as a sharp beam with smaller physical dimensions is urgently required.

Key words: Ultra-wideband (UWB); Antenna; Metamaterial
https://doi.org/10.1631/FITEE.1601193 **CLC number:** TN821

1 Introduction

Left-handed materials (LHMs) are increasingly being used in various applications because of their ability to modify the characteristics of the medium (Schantz, 2005). They are formed by periodic placement of the structures, such that each element has a size less than the wavelength of the medium. Thus, we can easily tune the characteristics of the medium by minor changes in the unit cell. They can be single negative materials (SNGs) or double negative materials (DNGs).

In this work, we use the Ansoft high-frequency structure simulator (HFSS) for the simulation of the designed structures. It uses the finite element method (FEM) for solving electromagnetic (EM) structures (Pozar, 1992).

In recent years, with the rapid development in wireless communications, various alphabetic metamaterial structures such as S-shaped, V-shaped, and U-shaped (Chen *et al*., 2004; Ekmekçi and Turhan-Sayan, 2007; Benosman and Hacene, 2012; Mallik *et al*., 2013), have been proposed to reduce the size of microstrip antennas. There has been ever-growing demands for antenna designs with compactness, low cost, high performance, and multi-band (Mahatthanajatuphat *et al*., 2009). With the use of fractal shapes of the radiating elements, multi-band resonance with a single antenna is becoming attractive (Gianvittorio and Rahmat-Samii, 2002).

‡ Corresponding author
ORCID: Parul DAWAR, http://orcid.org/0000-0003-4073-9013

2 Novel modified H-shaped split ring resonator metamaterial

The schematic and design parameters of the novel modified 'H-shaped' metamaterial (Islam *et al*., 2014) are shown in Fig. 1 and Table 1, respectively. It is composed of modified H-shaped resonating copper conductors placed between two modified SRR structures.

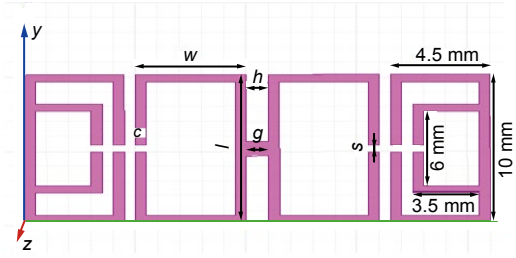

Fig. 1 Schematic of the novel modified H-shaped SRR metamaterial

Table 1 Design parameters of the novel modified H-shaped SRR metamaterial

Parameter	Value	Parameter	Value
l	10 mm	g	1 mm
s	0.5 mm	h	1 mm
c	1 mm	w	5 mm

The width of each outer split-square resonator is 0.5 mm, and the outer length is 10 mm with a 0.5 mm split. The structure is printed on a square-shaped Duroid substrate with a dielectric constant ε_r=2.2, a dielectric loss tangent $\tan\delta$=0.025, side length a= 25 mm, width b=14 mm, and thickness t=1.6 mm. The structure is placed between two waveguide ports (Fig. 2) at positive and negative locations on the x axis and excited by an electromagnetic wave in the direction of the x axis. The perfect electric conductor (PEC) boundary condition is applied to the y axis, and the z axis is defined as a perfect magnetic conductor (PMC) boundary.

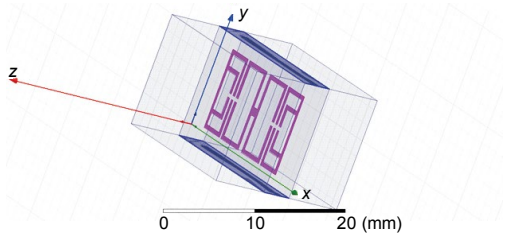

Fig. 2 Simulation setup for the novel metamaterial structure

The effective permeability and permittivity of the medium can be determined from the simulated complex S_{21} and S_{11} parameters using the Nicolson–Ross–Weir method (Ziolkowski, 2003). Figs. 3a–3c show the permittivity and permeability characteristics, and the S_{21} parameter (transmission coefficient).

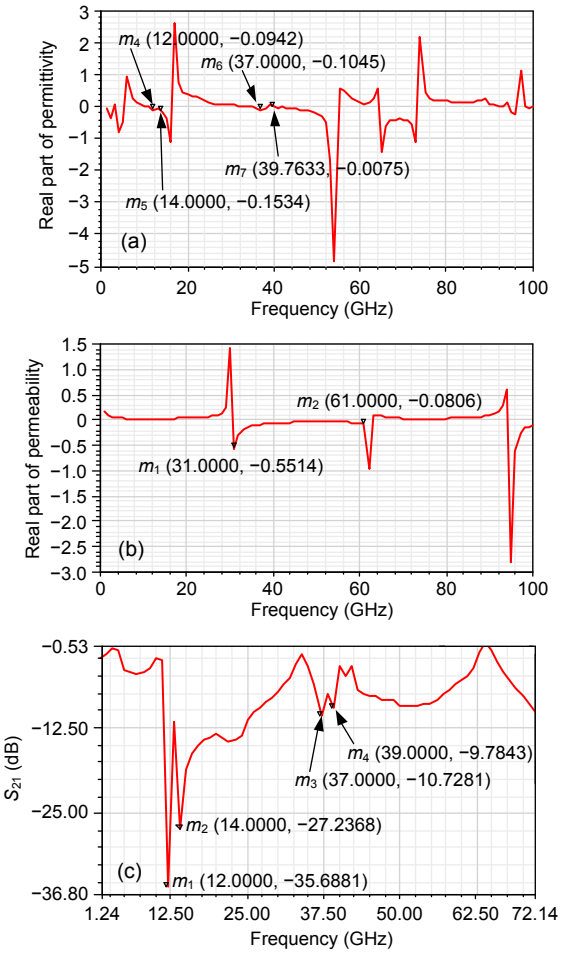

Fig. 3 Real part of permittivity (a), real part of permeability (b), and simulated transmission parameter (c)

It can be observed that the resonant frequencies of 12, 14, 37, and 39 GHz are obtained. Table 2 gives the values of permittivity, permeability, and S_{21} at the X, Ku, and Ka band frequencies.

Table 2 Real values of μ, ε, η, and S_{21}

Resonant frequency (GHz)	Re(μ)	Re(ε)	Re(η)
12	0.0262	−0.0942	2.8500
14	0.0320	−0.1534	−1.6035
37	−0.0873	−0.1045	−0.0052
39	−0.0656	0.0579	−0.4410

From Table 2, the negative refraction or double negative characteristics of the structure can be obtained at 37 GHz.

In metamaterial structures, the equivalent structure is obtained by calculating the resultant capacitance due to the gaps and the resultant inductance due to the metallic loops. This structure can be divided into three sections, as shown in Fig. 4 with its equivalent circuit.

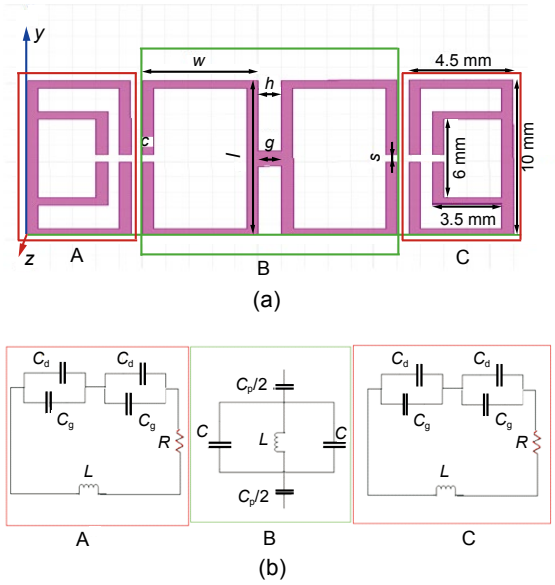

Fig. 4 Modified H-shaped SRR metamaterial (a) and equivalent circuit of the modified H-shaped SRR (b)

The three sections are joined by two gaps. According to the quasi-static theory, the capacitance in the gap is given by

$$C = \varepsilon_0 \varepsilon_r A / d, \tag{1}$$

where ε_0 and ε_r are the permittivity of free space and the relative permittivity, respectively, A is the cross-sectional area of the gap, and d is the gap length, which is s in our design.

The equivalent inductance and capacitance of section B is given by (Grover, 1946; Pendry *et al*., 1999; Paul, 2009)

$$L = \mu_0 t \left(\frac{2c}{2w+h} + \frac{\sqrt{(2w+h)^2 + l^2}}{c} \right), \tag{2}$$

$$C_p = \varepsilon_0 \left(\frac{2w+h}{\pi} \ln \frac{2c}{a-l} \right), \tag{3}$$

where the free-space permeability is $\mu_0=4\pi\times10^{-7}$ H/m and the free-space permittivity is $\varepsilon_0=8.85\times10^{-12}$ F/m.

Similarly, equivalent inductance and capacitance of sections A and B are given by (Saha and Siddiqui, 2011)

$$L_t = 0.0002\left[\lg(4l_w / d_w) - \theta\right], \tag{4}$$

$$2(l_r + w_r) = 2\pi r, \tag{5}$$

$$C_{gp} = \frac{C_{pul}}{2}\left(\pi \frac{L_{int} + w_{int}}{2\pi} - g + \frac{\varepsilon_0 wt}{2g} \right), C_{pul} = \frac{\sqrt{\varepsilon_e}}{c_0 Z_0}, \tag{6}$$

where subscript 'gp' stands for gap, subscript 'pul' stands for per unit length, θ=2.451, L_t is the total inductance, l_w is the length of the w strip, d_w is the depth of the w strip, l_r is the length of the outer ring (10 mm), and w_r is the width of the outer ring (4.5 mm), L_{int} and w_{int} are the length of the inner ring (3.5 mm) and width of the inner ring (6 mm) of the internal rectangular ring of the proposed SRRs' sections A and B (Fig. 1a), respectively, and ε_0 is the free-space permittivity. The split gap is 0.5 mm, and t and w are the thickness and width of rectangular rings, respectively. The capacitance C_{pul} denotes the capacitance per unit length between the rectangular rings, ε_e is the effective permittivity of the medium, $c_0=3\times10^8$ m/s is the speed of light in free space, and Z_0 is the impedance of the medium.

Upon substituting all the values, we obtain the resultant capacitance $C_{eq}=2\times10^{-13}$ F and resultant inductance $L_{eq}=7.3\times10^{-10}$ H. The resonant frequency of the unit cell can be calculated by

$$\omega = \sqrt{\frac{1}{L_{eq} C_{eq}}}. \tag{7}$$

The resonant frequency is found to be 13.17 GHz. Thus, there is a 6% error between the simulated and theoretical values of the resonant frequency of the metamaterial unit cell.

3 Microstrip patch antenna

Transmission line representation of the rectangular microstrip patch antenna is by two slots of width w and height h, separated by a transmission line of length l. It resonates at 32 GHz with dielectric

constant ε_r=2.2, substrate thickness h=3.2 mm, L=26.2 mm, and W=26.5 mm on a ground plane (Balanis, 1997). The ground plane is almost finite with a size greater than the patch by six times the substrate thickness, length L_g=65.6 mm, and width W_g=73 mm. Fig. 5 gives the constructional details.

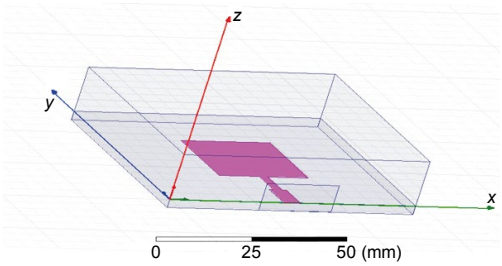

Fig. 5 Rectangular microstrip patch antenna

Microstrip feed using the quarter wave transformer feeds the antenna:

$$Z_{qw} = \sqrt{Z_{rmpa} \cdot Z_0}. \quad (8)$$

The input impedance Z_0 at the base of the microstrip feed line is 50 Ω. W_{qw} and L_{qw} represent the width (2.475 mm) and length (9.75 mm) of the quarter wave transformer as calculated from the impedance of the quarter wave transformer Z_{qw} using the TX line (transmission line calculator) software by AWR Corporation's Microwave Office. Fig. 6 shows the simulated return loss and radiation pattern in the H-plane of the rectangular microstrip patch antenna.

It can be seen that the return loss S_{11} is 32.59 dB at 32 GHz and the voltage standing wave ratio (VSWR) is 1.02. The bandwidth in the range of frequencies with VSWR<2 is 10 GHz. The peak gain is 9.7 dB and the peak directivity is 12.97 dB. It can be seen that the impedance of the antenna is around 90 Ω.

4 Proposed antenna configurations

To enhance the performance parameters of the antenna, three configurations are proposed, as shown in Fig. 7.

In Fig. 7b, the metamaterial is placed at a coupling distance of 0.5 mm from top of the patch in the middle of the substrate. The simulation results are shown in Fig. 8.

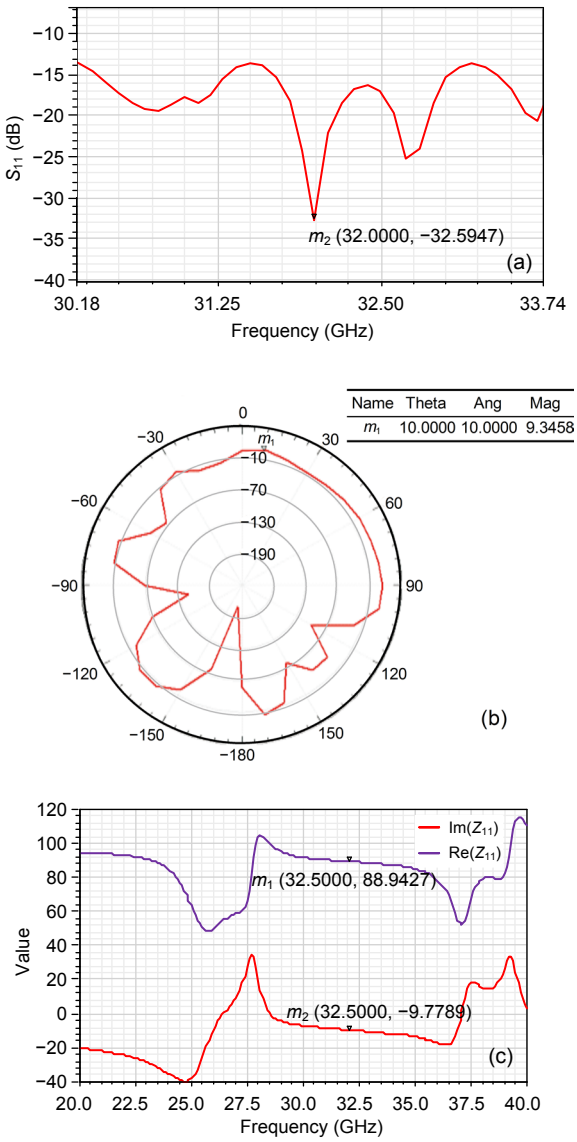

Fig. 6 Return loss (a), radiation pattern in the H-plane of RMPA (b), and real and imaginary parts of impedance vs. frequency in the patch antenna (c)

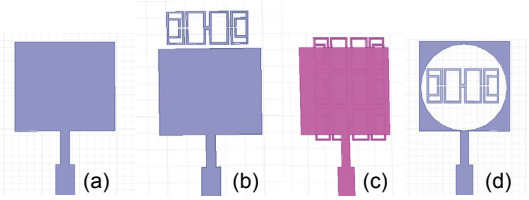

Fig. 7 Proposed antenna configurations: (a) patch antenna; (b) metamaterial placed at a coupling distance of 0.5 mm from top of the patch in the middle of the substrate; (c) metamaterial array formed with a 0.5 mm gap between each; (d) patch antenna with a lessened active area

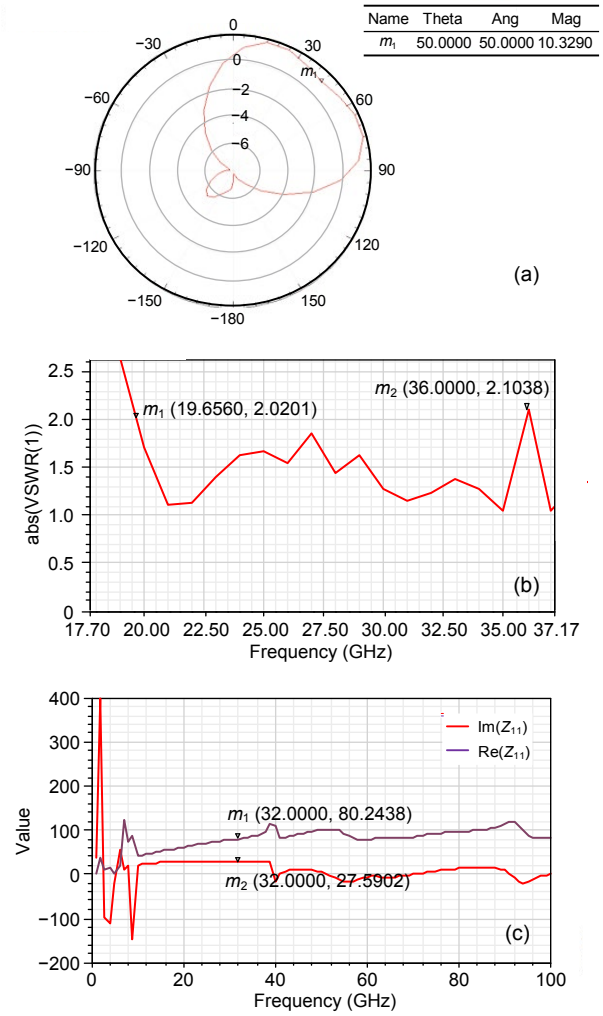

Fig. 8 Radiation pattern (a), VSWR (b), and impedance vs. frequency of the configuration in Fig. 7b (c)

In Fig. 7c, the metamaterial array, comprising three elements in a row, is formed with a 0.5 mm gap between each. The center of the array coincides with the center of the patch and is placed at the middle of the substrate. The simulation results are shown in Fig. 9.

The shifts in the resonant frequency are obtained at 9 and 18 GHz. This amounts to a miniaturization of the antenna structure by 71% and 43%, respectively.

The estimated expression for the exact bandwidth of a tuned antenna is inversely proportional to the magnitude $|Z'_0(\omega_0)|$ of the frequency derivative of the input impedance. It has been shown that a properly defined exact Q of a tuned lossy or lossless antenna is nearly proportional to $|Z'_0(\omega_0)|$, and thus Q is nearly inversely proportional to the bandwidth (for not too large a bandwidth) of a simply tuned antenna at all frequencies (Yaghjian and Best, 2005). Thus, by inserting the metamaterial array into the antenna substrate, the effective impedance decreaces, thereby increasing the bandwidth.

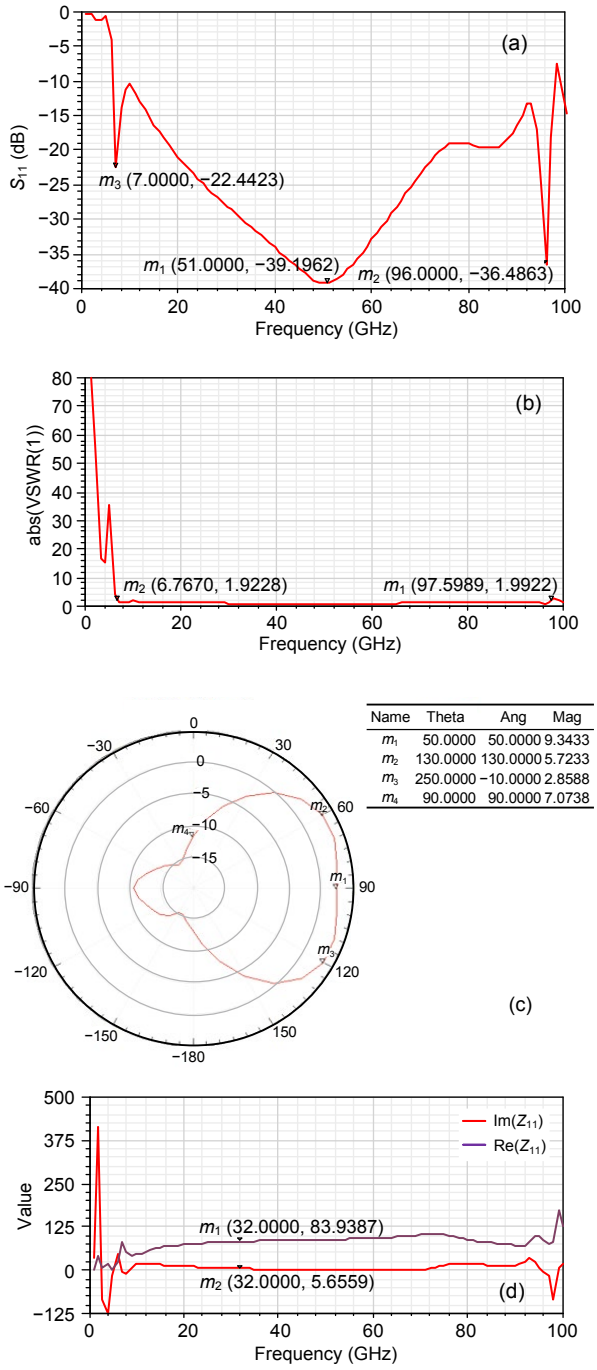

Fig. 9 Return loss curve (a), VSWR curve (b), radiation pattern (c), and impedance vs. frequency curve of the configuration in Fig. 7c (d)

In Fig. 9d, the rectangular patch antenna is shown with the active area reduced by the area of the circle of radius 12 mm. The active area (Saraswat and Kumar, 2016) is reduced by 65%. The metamaterial is placed in the middle of the substrate such that its center coincides with the center of the patch. The simulation results are shown in Fig. 10.

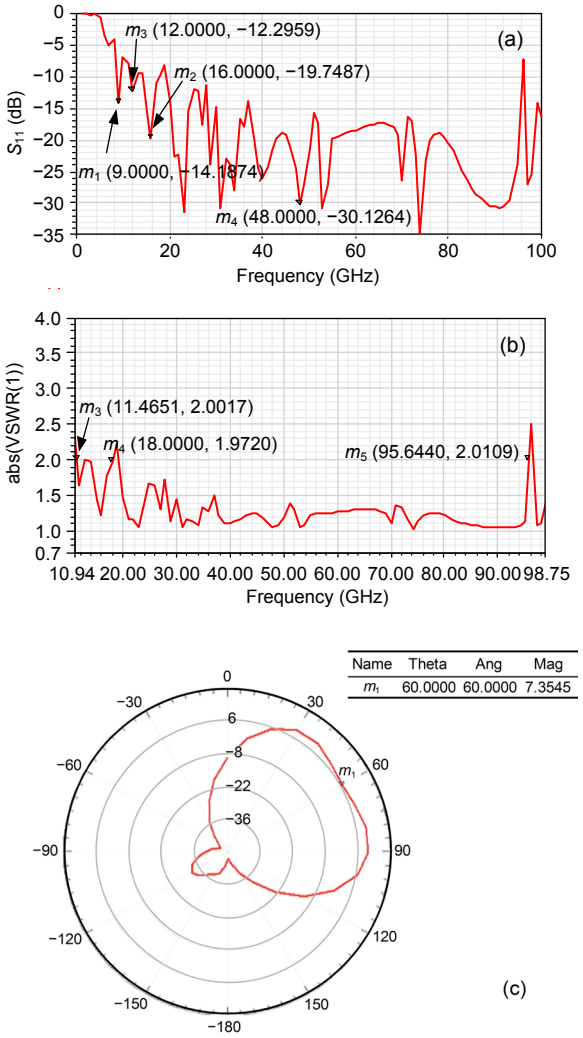

Fig. 10 Return loss curve (a), VSWR curve (b), and radiation pattern of the configuration in Fig. 7c (c)

Secondary resonances are obtained at 9, 12, and 18 GHz. This amounts to miniaturization of the antenna structure by 71%, 62.5%, and 43%, respectively. Fig. 11 shows the plot of Z_{11} in the operating frequency range of the antenna.

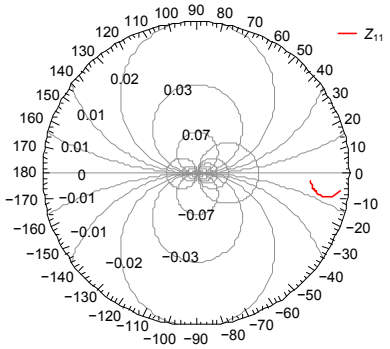

Fig. 11 Z_{11} in the operating frequency range of the antenna

We have the antenna impedance:

$$Z = \sqrt{L_{eq}/C_{eq}}. \tag{9}$$

The Smith chart explains the decrease in impedance, as the capacitive reactance is indicated by the curve. Thus, because of the capacitive loading of the antenna, the impedance decreases and the bandwidth increases.

The above results are summarized in Table 3.

From the above configurations, we first conclude that for high-directivity applications, the antenna must be coupled with the metamaterial on the top. This type of placement helps enhance the field in a particular direction. Second, for the ultra-wideband on the order of 91 GHz, the maximum miniaturization of 78% is achieved by the array of three metamaterials, where the center coincides with the center of the patch. This configuration leads to a decrease in the effective the bandwidth is enhanced. Third, the maximum medium characteristics just below the

Table 3 Results of different antenna configurations

Figure	Gain (dB)	Directivity (dB)	Radiation efficiency (%)	Bandwidth (GHz)	Return loss (dB)	Active area (mm^2)	Miniaturization (%)
Fig. 7a	9.7	12.97	73.0	10.00	32.59	694.3	–
Fig. 7b	10.0	10.40	97.4	16.34	23.28	694.3	71
Fig. 7c	9.7	9.40	99.5	91.00	39.19	694.3	78
Fig. 7d	8.7	7.40	100.0	77.00	30.12	241.9	71

patch. Hence, radiation efficiency with the maximum reduction in the active area of the patch can be obtained with a fractal antenna.

5 Fractal antenna

One method of reducing the antenna's active area is using the fractal geometry. Fractals are designed by some iterative mathematical formulae in such a way that the fractal is generated from any simple object (Fig. 12).

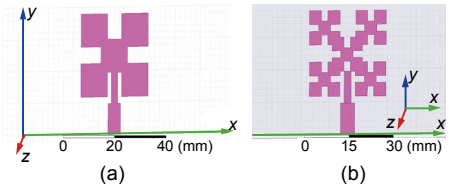

Fig. 12 Fractal of the first order (a) and second order(b)

In Fig. 12a, five fractals of dimensions 10.5 mm×10.5 mm are placed to form the first-order fractal antenna, and in Fig. 12b, each unit is further divided using the same iterative method to form the second-order fractal antenna.

The metamaterial, as a single element and as an array of three elements, is placed in the middle of the substrate such that the center of metamaterial coincides with the center of the patch for both first- and second-order fractals (Fig. 13). The results obtained have been tabulated in Table 4.

In the configuration of Fig. 13a, high directivity is achieved because of the operation in the near-zero-refraction region. As the refraction is very close to 0 or very much less than 1, the field lines are highly directed (Fig. 14).

Thus, using the fractal metamaterial antenna of second-order iterative mathematics, we can

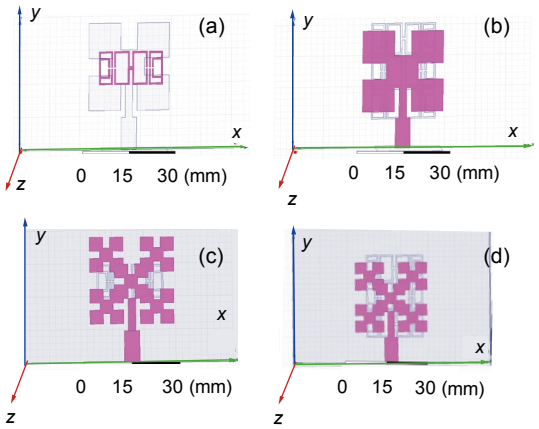

Fig. 13 Fractal metamaterial antenna: (a) first-order fractal antenna with metamaterial; (b) first-order fractal antenna with a metamaterial array; (c) second-order fractal antenna with metamaterial; (d) second-order fractal antenna with a metamaterial array

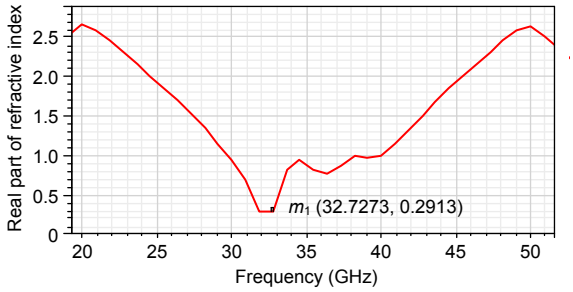

Fig. 14 Real part of the refractive index vs. frequency

miniaturize the antenna by 21 times along with the improvement in bandwidth. The miniaturization is possible because the perimeter of the patch increases with the order of fractalization. The increase in bandwidth is achieved because of the decrease in impedance of the substrate. This is a boon in today's wireless communication, where a very sharp resonance antenna with smaller physical dimensions is required.

Table 4 Fractal metamaterial antenna

Figure	Gain (dB)	Directivity (dB)	Radiation efficiency (%)	Bandwidth (GHz)	Return loss (dB)	Miniaturization
Fig. 12a	8.88	8.94	98.70	12.41	31.18	–
Fig. 13a	10.23	10.26	99.28	16.59	26.32	7%
Fig. 13b	8.90	8.90	98.90	20.00	28.80	–
Fig. 12b	7.00	7.00	98.00	17.50	23.50	1/4 at 6.3 GHz
Fig. 13c	7.00	7.00	98.00	41.40	31.00	1/21 at 1.5 GHz
Fig. 13d	7.00	7.00	97.00	34.00	20.00	1/5 at 6.0 GHz

6 Results and discussion

In this paper, two techniques have been proposed to realize a miniaturized patch antenna as follows:

1. A circular slot has been cut from the rectangular patch, which reduces the active area of the patch.

2. The fractalization approach leads to a reduction in the active patch area and volume of the antenna structure.

Many sizes and shapes are used for designing the fractal antennas (Barasara *et al*., 2012).

Fractal antennas have been extensively used in wireless communication as they can fit into a small space and have multiple frequencies of operation (Cohen, 1997; Vinoy, 2002; Singh *et al*., 2009). When the order of iterations in the antenna increases, the size decreases and the effective electrical length increases, which leads to the miniaturization of the antenna (Cohen, 1995; Best and Morrow, 2002). As the volume decreases, the energy can be coupled more efficiently from the feed line.

The above miniaturization techniques have been combined with the use of metamaterials to improve the bandwidth of the patch antenna. For example, the metamaterial cover increases gain, bandwidth, and directivity (Harrington, 1960; Gupta, 1988; Dwivedi *et al*., 2013; Nordin *et al*., 2013), it increases directivity by focusing more energy, and it (SRR, etc.) reduces surface waves. Size reduction (63%) of the patch can be achieved by using metamaterials, e.g., a mushroom structure (CRLH-TL). In addition, a wider band can be obtained by reducing the ground plane of the antenna. An ultra-wideband (189%) can be achieved by placing a number of metamaterial unit cells.

In this study, using different metamaterial orientations and shapes of the antenna, the bandwidth has been increased by nine times, and the second-order fractal metamaterial antenna helps achieve high miniaturization of the order of 1/21, which is the largest achieved so far.

7 Conclusions

A new double-negative metamaterial unit cell structure was presented that resonates at frequencies in the X, Ku, and Ka bands of the microwave spectra. The latter band has wide applications in microspacecraft development. By using different metamaterial orientations and shapes of the antenna, bandwidth was increased by nine times, and miniaturization of 78% and 62.5% in the active area of the patch antenna was achieved. The new metamaterial antenna with reduced active area promises a 100% radiation efficiency with a little compromise between gain and directivity. The second-order fractal metamaterial antenna helps achieve high miniaturization of the order of 1/21. This is truly a boon in communication, as a sharp beam with smaller physical dimensions is highly desired.

References

Balanis, C.A., 1997. Antenna Theory. John Wiley & Sons, Inc., New York.

Barasara, D.J., Prajapati, J.C., Dethalia, A.M., 2012. Multi-frequency fractal antenna. *Int. J. Sci. Eng. Res.*, **3**(7):1-3.

Benosman, H., Hacene, N.B., 2012. Design and simulation of double "S" shaped metamaterial. *Int. J. Comput. Sci*., **9**(2):534-537.

Best, S.R., Morrow, J.D., 2002. The effectiveness of space-filling fractal geometry in lowering resonant frequency. *IEEE Antennas Wirel. Propag. Lett.*, **1**:112-115. https://doi.org/10.1109/LAWP.2002.806050

Chen, H.S., Ran, L.X., Huangfu, J.T., *et al*., 2004. Left-handed materials composed of only S-shaped resonators. *Phys. Rev. E*, **70**(5):057605. https://doi.org/10.1103/PhysRevE.70.057605

Cohen, N., 1995. Fractal antennas part-1: introduction and the fractal Quad. *Commun. Quat. Summ.*, p.7-22.

Cohen, N., 1997. Fractal antenna applications in wireless telecommunications. Proc. Electronic Industries Forum of New England, p.43-49. https://doi.org/10.1109/EIF.1997.605374

Dwivedi, S., Mishra, V., Kosta, Y.P., 2013. Design and Comparative analysis of a metamaterial included slotted patch antenna with a metamaterial cover over patch. *Int. J. Recent Technol. Eng.*, **1**(6):37-41.

Ekmekçi, E., Turhan-Sayan, G., 2007. Investigation of effective permittivity and permeability for a novel V-shaped metamaterial using S-parameters. Proc. 5th Int. Conf. on Electrical and Electronics Engineering, p.5-9.

Gianvittorio, J.P., Rahmat-Samii, Y., 2002. Fractal antennas: a novel antenna miniaturization technique, and applications. *IEEE Antennas Propag. Mag.*, **44**(1):20-36. https://doi.org/10.1109/74.997888

Grover, F.W., 1946. Inductance Calculations: Working Formulas and Tables. Dover Publication, Inc., New York, USA.

Gupta, K.C., 1988. Broadbanding Technique for Microstrip Patch Antennas: a Review. Technical Report No. 98,

University of Colorado, CO.

Harrington, R.F., 1960. Effect of antenna size on gain, bandwidth, and efficiency. *J. Res. Nat. Bur. Stand. D: Radio Propag.*, **64D**(1):1. https://doi.org/10.6028/jres.064D.003

Islam, S.S., Faruque, M.R.I., Islam, M.T., 2014. The design and analysis of a novel split-H-shaped metamaterial for multi-band microwave applications. *Materials*, **7**(7): 4994-5011. https://doi.org/10.3390/ma7074994

Mahatthanajatuphat, C., Saleekaw, S., Akkaraekthalin, P., *et al*., 2009. A rhombic patch monopole antenna with modified Minkowski fractal geometry for UMTS, WLAN, and mobile WIMAX application. *Prog. Electromagn. Res.*, **89**:57-74. https://doi.org/10.2528/PIER08111907

Mallik, A., Kundu, S., Goni, M.O., 2013. Design of a novel two-rectangular U-shaped double negative metamaterial. Int. Conf. on Informatics, Electronics & Vision, p.1-6. https://doi.org/10.1109/ICIEV.2013.6572646

Nordin, M.A.W., Islam, M.T., Misran, N., 2013. Design of a compact ultrawideband metamaterial antenna based on the modified split-ring resonator and capacitively loaded strips unit cell. *Prog. Electromagn. Res.*, **136**:157-173. https://doi.org/10.2528/PIER12100708

Paul, C.R., 2009. Inductance: Loop and Partial. Wiley-IEEE Press, New Jersey, USA.

Pendry, J.B., Holden, A.J., Robbins, D.J., *et al*., 1999. Magnetism from conductors and enhanced nonlinear phenomena. *IEEE Trans. Microw. Theory Technol.*, **47**(11): 2075-2084. https://doi.org/10.1109/22.798002

Pozar, D.M., 1992. Microstrip antennas. *Proc. IEEE*, **80**(1): 79-91. https://doi.org/10.1109/5.119568

Saha, C., Siddiqui, J.Y., 2011. Versatile CAD formulation for estimation of the resonant frequency and magnetic polarizability of circular split ring resonators. *Int. J. RF Microw. Comput. Aided Eng.*, **21**(4):432-438. https://doi.org/10.1002/mmce.20533

Saraswat, R.K., Kumar, M., 2016. Miniaturized slotted ground UWB antenna loaded with metamaterial for WLAN and WiMAX applications. *Prog. Electromagn. Res. B*, **65**:65-80. https://doi.org/10.2528/PIERB15112703

Schantz, H., 2005. The Art and Science of Ultra-Wideband Antennas. Artech House Publishers.

Singh, K., Grewal, V., Saxena, R., 2009. Fractal antennas: a novel miniaturization technique for wireless communications. *Int. J. Recent Trends Eng.*, **2**(5):172-176.

Vinoy, K.J., 2002. Fractal Shaped Antenna Elements for Wide- and Multi-band Wireless Applications. PhD Thesis, The Pennsylvania State University, Pennsylvania, USA.

Yaghjian, A.D., Best, S.R., 2005. Impedance, bandwidth, and *Q* of antennas. *IEEE Trans. Antennas Propag.*, **53**(4): 1298-1324. https://doi.org/10.1109/TAP.2005.844443

Ziolkowski, R.W., 2003. Design, fabrication, and testing of double negative metamaterials. *IEEE Trans. Antennas Propag.*, **51**(7):1516-1529. https://doi.org/10.1109/TAP.2003.813622